Estimation of Wiebe Function Parameters for Syngas and Anode Off-Gas Combustion in Spark-Ignition Engines

Ruinan Yang
Department of Mechanical Engineering,
Stony Brook University,
113 Light Engineering, 100 Nicolls Road,
Stony Brook, NY 11794

Zhongan Ran
Department of Mechanical Engineering,
Stony Brook University,
113 Light Engineering, 100 Nicolls Road,
Stony Brook, NY 11794

Dimitris Assanis
ASME Mem.
Department of Mechanical Engineering,
Stony Brook University,
131 Light Engineering, 100 Nicolls Road,
Stony Brook, NY 11794
e-mail: dimitris.assanis@stonybrook.edu

Wiebe functions, analytical equations that estimate the fuel mass fraction burned (MFB) during combustion, have been effective at describing spark-ignition (SI) engine combustion using gasoline fuels. This study explores if the same methodology can be extended for SI combustion with syngas, a gaseous fuel mixture composed of H_2, CO, and CO_2, and anode-off gas; the latter is an exhaust gas mixture emitted from the anode of a Solid Oxide Fuel Cell, containing H_2, CO, H_2O, and CO_2. For this study, anode off-gas is treated as a syngas fuel diluted with CO_2 and vaporized water. Combustion experiments were run on a single-cylinder, research engine using syngas and anode-off gas as fuels. One single Wiebe function and three double Wiebe functions were fitted and compared with the MFB profile calculated from the experimental data. It was determined that the SI combustion process of both the syngas and the anode-off gas could be estimated using a governing Wiebe function. While the detailed double Wiebe function had the highest accuracy, a reduced double Wiebe function is capable of achieving comparable accuracy. On the other hand, a single Wiebe function is not able to fully capture the combustion process of a SI engine using syngas and anode off-gas. [DOI: 10.1115/1.4056856]

Introduction

Spark ignition (SI) combustion is generally used on light-duty engines from the last century. In spite of its widespread use and development, the improvement in SI engine thermal efficiency is still limited due to the knock-limited compression ratio and operation with a stoichiometric air–fuel mixture. However, lean, low-temperature combustion is able to achieve higher thermal efficiency with low NOx emissions. When the engine operates in a lean condition, more complete combustion occurs in the cylinder, thus yielding high combustion efficiency due to the presence of excess oxygen. Ultimately, when the air–fuel ratio keeps increasing, the combustion efficiency and thermal efficiency drop due to a reduction of laminar flame speed and the occurrence of misfires [1,2]. Since engine performance is limited at very lean combustion conditions, it is necessary to find a fuel that can operate at an extended lean equivalence ratio range.

Alternative fuels, such as natural gas, methanol, and ethanol, have proven to be acceptable substitutes to gasoline for transportation applications. They have been shown to extend lean misfire limits compared to gasoline, which is typically confined to a narrow range of air–fuel ratios [3]. Synthesis gas, or syngas, is a gaseous fuel that can be produced from natural gas reforming, gasification of coal, hydrocarbon raw material, and alkaline electrolysis of water [4]. Syngas is a fuel consisting of a mixture of H_2 and CO at varying volume ratios. Due to the lower density of H_2 and CO, syngas has a lower heating value (LHV) than conventional liquid and gaseous hydrocarbon fuels [5]. Since H_2 has a high laminar flame speed and low ignition energy requirement, a SI engine fueled with syngas can achieve a wider range of lean operating conditions than gasoline [6,7]. Syngas is also able to operate at a higher compression ratio compared with gasoline fuel, as a result of its higher octane rating, which can contribute to achieving a higher thermal efficiency [8]. Since syngas does not include hydrocarbons, the unburned hydrocarbon emissions are significantly reduced in SI combustion fueled with syngas. Meanwhile, lean SI combustion results in lower in-cylinder combustion temperatures, thus reducing NOx emissions, as well. However, the engine volumetric efficiency and output power are significantly reduced using syngas as the fuel, due to its gaseous state nature.

Over the past several years, scientists have been working on studying the fuel properties, performance, and operating ranges of syngas SI combustion. Sridhar and Yarasu [9] demonstrated that a higher compression ratio can result in higher thermal efficiency with syngas combustion. However, as the compression ratio increases, the efficiency benefit is reduced. A similar result was demonstrated by Ran et al. [10,11], in comparisons between syngas, compressed natural gas, and ethanol. Mustafi et al. [12] computationally evaluated syngas combustion performance and related emissions. Bika et al. [13] analyzed combustion under different H_2 to CO ratios. The results showed that the maximum thermal efficiency was achieved at an H_2 to CO ratio of 1. Dai et al. [14] showed that SI combustion of gasoline with syngas addition at 2.5% achieved the maximum thermal efficiency. Shah et al. [15] demonstrated that the CO and NOx emissions of syngas were lower than gasoline with similar efficiency.

The solid oxide fuel cell (SOFC) is an electrochemical conversion device that generates electricity by oxidizing fuel directly, without combustion. It has a high conversion efficiency and low emissions of pollutants [16,17]. A SOFC can be coupled with an internal combustion engine (ICE) that is fueled with the highly diluted SOFC anode off-gas to generate additional power from this hybrid arrangement. Compared with the common SOFC–gas turbine systems, SOFC–ICE is able to accomplish high system efficiency for lower power generation range applications [18].

The anode off-gas harvested from the SOFC anode consists of H_2, CO, CO_2, and H_2O, which can be treated as a syngas fuel diluted with CO_2 and water. Some research has been done previously investigating the benefits of hybridizing SOFCs with ICE. Fyffe et al. [19] developed a model for a SOFC and an ICE as a quick-start hybrid system to achieve high efficiency. The results showed that the theoretical exergy efficiency was close to 70%. Additionally, an experimental study of anode off-gas using spark-assisted ignition was also conducted by Kim et al. [20], which

Manuscript received September 29, 2022; final manuscript received January 27, 2023; published online February 27, 2023. Editor: Jerzy T. Sawicki.

showed that thermal efficiency of up to 61.6% could be achieved. Ran et al. [21] also illustrated that the anode off-gas SI combustion can achieve a similar thermal efficiency with lower NO_x and hydrocarbon emissions compared with compressed natural gas over a certain range of air–fuel ratios.

To accelerate the development of SI engines using syngas and anode off-gas as potential fuels, a better understanding and description of their heat release characteristics is required. Such heat release models can be embedded in one-dimensional (1D) system-level engine models to study the effect of engine geometry and operating conditions on engine performance and fuel efficiency. While 1D models cannot predict spatially resolved details of combustion and pollutant formation processes in the cylinder, they can be used effectively for engine and system design studies with acceptable computational time and without requiring chemical mechanisms.

In order to describe the fraction of the total heat released during the SI combustion process, referred to as the mass fraction burned [22], a Wiebe function is employed. The Wiebe function can generate an S-shaped curve from 0 to 1, which in this case, can represent the start and end of combustion. Previous researches have shown that a single Wiebe function can be used to accurately describe heat release in a SI combustion model [23,24]. Shivapuji and Dasappa [25] had created a Wiebe function for an SI engine fueled with producer gas. Carrera et al. [26] estimated the Wiebe function for a SI engine using biogas as the fuel. However, the original single Wiebe function cannot capture the combustion process precisely when a fuel provides more than one stage of heat release. Since a single Wiebe function was not able to predict both the combustion near the core and the combustion close to the boundary, a function that could predict more complex combustion was required for engine study.

A double Wiebe function includes premixed combustion and diffusion combustion stages and is typically used for estimation of compression ignition (CI) combustion. Double Wiebe functions can also be used for advanced combustion modes and even SI combustion with fuel that exhibits two-stage heat release characteristics. A double Wiebe function was introduced by Ghojel [27], who proposed a model for direct injection CI combustion engines. Yasar et al. [28] created a single-zone, double Wiebe function for homogeneous charge compression ignition (HCCI) combustion. Similar work was also conducted by Aziz and Heikal [29], who used a double Wiebe function to describe a dual fuel HCCI combustion. Meanwhile, Yeliana et al. [30] estimated a double Wiebe function for a SI engine fueled with ethanol–gasoline blends. Liu and Dumitrescu [31] compared the single and double Wiebe functions for a natural gas SI engine.

In this study, a single Wiebe function and three double Wiebe functions were fitted using heat release rates calculated from experimental results [10,11,21,32]. The Wiebe functions were incorporated into a 1D system-level model as alternatives to model combustion of a SI engine fueled with syngas and anode off-gas. The model was validated against experimental data to confirm its accuracy. In particular, the predicted cylinder pressure using a Wiebe function was compared with the corresponding experimental measured pressure profiles. The Wiebe function with both high accuracy and acceptable computation time would be selected as the best choice to capture the combustion process for both syngas and anode off-gas SI combustion. Using this methodology, the 1D model could be used for design studies of SI engines fueled with syngas and anode off-gas.

Table 1 CFR engine specifications

Bore (mm)	82.6
Stroke (mm)	114.3
Connecting rod (mm)	254
Compression ratio	6:1–18:1
Encoder shaft resolution (CAD)	0.2
Intake valve opening (deg aTDC)	−350
Intake valve closing (deg aTDC)	−146
Exhaust valve opening (deg aTDC)	140
Exhaust valve closing deg (aTDC)	−345

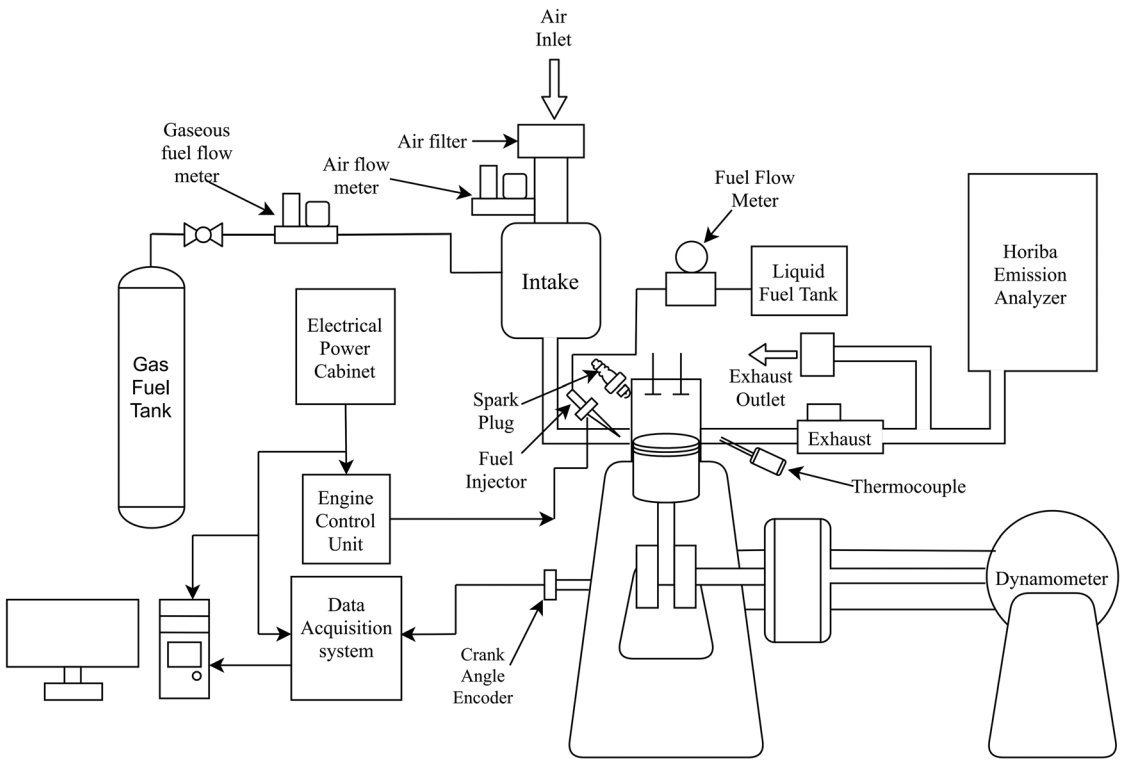

Fig. 1 Schematic of experiment setup [10]

Table 2 Fuel properties for syngas and anode off-gas [10,11,21,32]

Fuels	Syngas	Anode off-gas
Formula	$C_{0.410}H_{1.181}O_{0.410}$	$C_{0.66}H_{0.68}O_{1.16}$
MW (g/mol)	12.7	27.16
H/C Ratio	2.88	1.03
LHV (MJ/kg)	20.5	4.69
Stoich AFR	5.4	1.26

Experimental Setup and One-Dimensional System-Level Model

Experimental Setup. The experiments were conducted on a single-cylinder, four-stroke Cooperative Fuel Research (CFR) spark ignition engine. The engine specifications are shown in Table 1. Figure 1 illustrates the schematic of the CFR engine. The speed and torque of the engine were measured by a direct current (DC) dynamometer, which was mounted next to the engine. The intake air came into the intake system through an air filter and the air flowrate was controlled by an Alicat MCRW-500SLPM-D/5M flowmeter. The gaseous fuel was injected into the plenum and controlled by an Alicat MCRW-100SLPM-D/5M flowmeter. The crankshaft position was determined by a BEI XH25D-SS-1024 encoder with a resolution of 0.2 crank angle degrees. The cylinder pressure was measured by a Kistler 7061B pressure transducer. The emissions were measured by a Horiba MEXA-7100DEGR exhaust gas analyzer. The air–fuel ratio was controlled and measured by a Bosch LSU lambda sensor. The engine spark timing was controlled using an engine control unit and experimental data was collected through a data acquisition system created in LabVIEW.

The engine speed was operated at a constant speed of 1200 rpm, with the intake pressure and temperature set at 75 kpa and 300 K. Two-hundred cycles of cylinder pressure data were collected during the combustion for each data point. The compression ratio was varied between 8:1 and 11:1 for syngas, and 11:1 and 13:1 for anode off-gas. Each dataset was collected at the maximum brake torque timing by changing the spark timing. The syngas used in this experiment contained 60% H_2 and 40% CO, while the anode off-gas contained 33.9% H_2, 15.6% CO, and 50.5% CO_2. The anode off-gas generated from the SOFC–ICE was highly diluted with water vapor, which significantly decreased the energy content of the fuel. In order to eliminate the negative effect on combustion, the water vapor was removed from the anode off-gas. The fuel properties for syngas and anode off-gas are shown in Table 2.

One-Dimensional System-Level Model. A 1D system-level simulation model was created using a commercial, 1D engine system software AVL BOOST [33]. The cylinder model is constructed based on the zero-dimensional approach, and the pipe model is created based on the 1D fluid dynamic calculation. The engine geometry and the valve timings were measured from the experimental setup. The operating conditions of the experiments were used in the model. The heat release fraction during the actual combustion process was calculated from the experimental data and then used in the model as the input MFB curve. Figure 2 illustrates the validation of the cylinder pressure between the experimental data and the simulation results, and the apparent heat release rate. The legend Exp stands for the experimental results and Sim stands for the simulation results, which will also be used in the following figures. The comparison shows that this 1D model is able to capture the combustion process of an SI engine fueled with syngas and anode off-gas and it could be used for further thermodynamic studies.

As previously state in the Introduction section, the Wiebe function is used to estimate the MFB, which is the ratio between the burned fuel and the total fuel inducted into the combustion chamber. Equation (1) shows the equation for the single Wiebe function

$$x_b(\theta) = 1 - \exp\left[-a\left(\frac{\theta-\theta_0}{\Delta\theta}\right)^{m+1}\right] \tag{1}$$

where $x_b(\theta)$ is the fraction of fuel burned, θ is the crank angle, θ_0 is the start of combustion, $\Delta\theta$ is the combustion duration, m is the form factor, and a is the efficiency parameter.

The double Wiebe function includes two standard Wiebe functions, which stand for premixed combustion and diffusion combustion. A weight factor is defined to determine the fraction of each stage. Equation (2) illustrates the form of the double Wiebe function

$$\begin{aligned} x_b(\theta) = {} & \lambda\left\{1 - \exp\left[-a_1\left(\frac{\theta-\theta_0}{\Delta\theta_1}\right)^{m_1+1}\right]\right\} \\ & + (1-\lambda)\left\{1 - \exp\left[-a_2\left(\frac{\theta-\theta_0}{\Delta\theta_2}\right)^{m_2+1}\right]\right\} \end{aligned} \tag{2}$$

where λ is the weight factor, 1,2 is the combustion stage 1 and 2, which refers to the premixed combustion and diffusion combustion, respectively.

In the following sections, this double Wiebe function is referred to as a detailed double Wiebe function (DDWF).

In order to reduce the number of coefficients for the double Wiebe function, two reduced double Wiebe functions are considered in this study. Equation (3) shows the first reduced double Wiebe function, which defines the form factor m as the same value for both stages; and Eq. (4) defines the efficiency factor as the same value for both stages. Equations (3) and (4) are shown below and are called reduced double Wiebe function-form factor (RDWF-form factor) and reduced double Wiebe function-efficiency factor (RDWF-efficiency factor) in the following sections.

$$\begin{aligned} x_b(\theta) = {} & \lambda\left\{1 - \exp\left[-a_1\left(\frac{\theta-\theta_0}{\Delta\theta_1}\right)^{m+1}\right]\right\} \\ & + (1-\lambda)\left\{1 - \exp\left[-a_2\left(\frac{\theta-\theta_0}{\Delta\theta_2}\right)^{m+1}\right]\right\} \end{aligned} \tag{3}$$

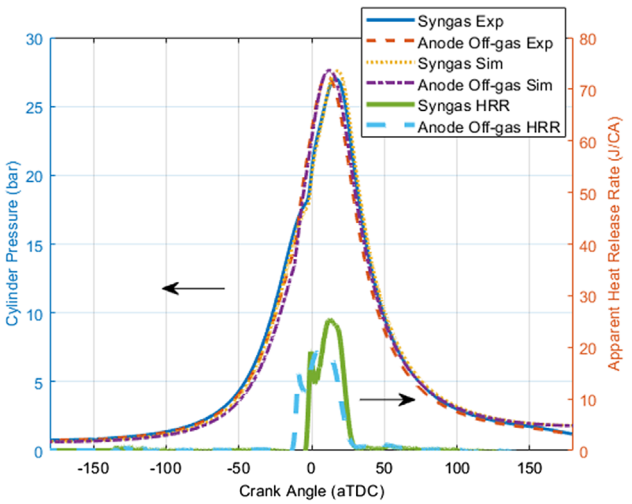

Fig. 2 Model validation

$$x_b(\theta) = \lambda\left\{1 - \exp\left[-a\left(\frac{\theta-\theta_0}{\Delta\theta_1}\right)^{m_1+1}\right]\right\} + (1-\lambda)\left\{1 - \exp\left[-a\left(\frac{\theta-\theta_0}{\Delta\theta_2}\right)^{m_2+1}\right]\right\} \quad (4)$$

The Wiebe function was fitted against the cumulative heat release calculated from the experiment data, which was the ratio between the cumulative energy released and total energy input. In this paper, the least square method (LSM) was used to estimate the coefficient of the Wiebe functions. The root-mean-square error (RMSE) was calculated using Eq. (5) and it was used to determine the accuracy of the fitting result. By comparing the RMSE and the complexity of the equation, a suitable Wiebe function would be selected to describe the combustion of both syngas and anode off-gas. The predicted combustion profile was used in the 1D thermodynamic model and the cylinder pressure generated from the model was compared with the measured pressure to verify the accuracy of the model. Figure 3 shows the stages of this modeling study.

$$\text{RMSE} = \sqrt{\frac{1}{n}\sum_{1}^{n}(y_p - y_r)^2} \quad (5)$$

Results and Discussion

Mass Fraction Burned. In this section, 12 groups of experimental data collected from previous research [10,11,21] were selected to estimate and validate the MFB created from the Wiebe functions. The operation condition was intake pressure 75 kpa, intake temperature 300 K, equivalence ratio between 0.4 to 0.9 and no EGR. Table 3 presents the information of all data points.

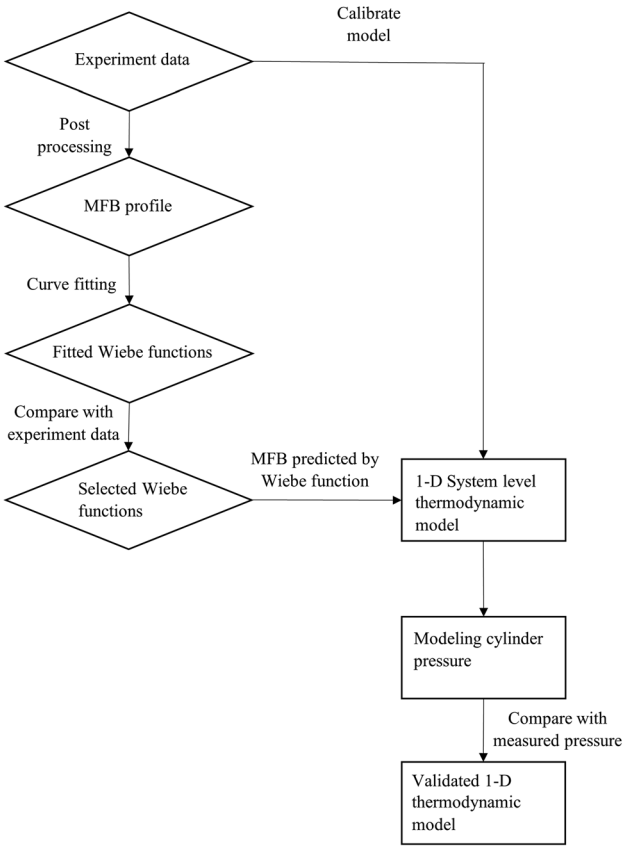

Fig. 3 Flow chart of the 1D thermodynamic model

More detailed operation condition and combustion timing were illustrated in Appendix B. For different compression ratios and different types of fuels, three groups of data with varying spark timing were used to fit the Wiebe function using the calculated normalized heat release combustion profile from the experimental data, and one group of data was used to validate the fitted results.

The start of combustion for the single Wiebe function was determined by calculating the crank angle degree of 0% heat release in the experiment, which was shown as CA0. The combustion duration was stated by the crank angle between 0% and 100% of the total energy released during combustion in one cycle. Due to the limitation of measurement error during experiments, it was not easy to determine the exact crank angle position of 100% heat release; hence, the crank angle degree corresponding to 95% of the fuel burned in the cylinder was used to denote the end of the combustion. Table 4 illustrates the coefficients and Eq. (6) shows the fitted result of the single Wiebe function. The RMSE between the experimental heat release and the single Wiebe function is 7.3%. From Table 4 it can be seen that the difference of the coefficients between syngas and anode off-gas are quite large, which means a single Wiebe function cannot be used to capture the combustion process of both syngas and anode off-gas simultaneously

$$x_b(\theta) = 1 - \exp\left[-4.26\left(\frac{\theta-\theta_0}{\Delta\theta}\right)^{1.01+1}\right] \quad (6)$$

A double Wiebe function consists of two heat release stages, as described previously. The start of combustion of these two stages was assumed to be the CA0 for both. The end of premixed combustion was defined by fitting the function using the LSM, and the end of diffusion combustion was defined by the CA95. The detailed double Wiebe function is shown in Eq. (7) and the coefficients for each operating point are listed in Table 5. The average RMSE of this detailed double Wiebe function was 1.2%, which is significantly smaller than the single Wiebe function. Unlike the single Wiebe function, the coefficients for syngas and anode off-gas are similar in magnitude, which means the detailed double Wiebe function can be used to capture the combustion process of both syngas and anode off-gas for the operating conditions evaluated in this study.

$$x_b(\theta) = 0.29\left\{1 - \exp\left[-2.22\left(\frac{\theta-\theta_0}{\Delta\theta_1}\right)^{0.16+1}\right]\right\} + 0.71\left\{1 - \exp\left[-2.94\left(\frac{\theta-\theta_0}{\Delta\theta_2}\right)^{2.21+1}\right]\right\} \quad (7)$$

Equations (8) and (9) illustrate two reduced double Wiebe functions assuming the same form factor and efficiency factor for the two standard Wiebe functions, respectively. The RMSE for

Table 3 Compression ratio and fuel type for all operation points

Data	Compression ratio	Fuel type	Use
1	9	Syngas	Fit
2	9	Syngas	Fit
3	9	Syngas	Fit
4	11	Syngas	Fit
5	11	Syngas	Fit
6	11	Syngas	Fit
7	11	Anode off-gas	Fit
8	11	Anode off-gas	Fit
9	11	Anode off-gas	Fit
10	9	Syngas	Validate
11	11	Syngas	Validate
12	11	Anode off-gas	Validate

Table 4 Coefficients for single Wiebe function

Coefficients	a	m
Data 1	8.83	1.14
Data 2	6.50	1.19
Data 3	3.14	1.18
Data 4	3.16	0.98
Data 5	3.10	0.96
Data 6	3.12	0.97
Data 7	3.62	0.90
Data 8	3.45	0.87
Data 9	3.42	0.91

Table 5 Coefficients for detailed double Wiebe function

	λ	a_1	m_1	a_2	m_2
Data 1	0.33	2.39	0.11	4.75	2.54
Data 2	0.28	2.71	0.21	3.94	2.48
Data 3	0.28	1.94	0.25	2.45	2.50
Data 4	0.28	2.17	0.11	2.51	2.23
Data 5	0.30	2.07	0.17	2.45	2.21
Data 6	0.30	1.99	0.21	2.43	2.15
Data 7	0.28	2.29	0.13	2.73	1.97
Data 8	0.29	2.23	0.13	2.64	1.92
Data 9	0.28	2.18	0.12	2.61	1.93

Eq. (8) is 1.5%, and 1.2% for Eq. (9). Both these two reduced Wiebe functions resulted in a lower RMSE compared with the single Wiebe function. The double Wiebe functions with the reduced efficiency factor achieved a similar accuracy as the detailed double Wiebe function, as shown in Eq. (7). Tables 6 and 7 list the coefficients for the two reduced double Wiebe functions. Like the detailed double Wiebe function, the difference in the value of the coefficients between syngas and anode off-gas combustion is minimal. Table 8 shows the RMSE for data 10–12 of single and double Wiebe functions

$$x_b(\theta) = 0.13\left\{1 - \exp\left[-8.64\left(\frac{\theta-\theta_0}{\Delta\theta_1}\right)^{1.66+1}\right]\right\} + 0.87\left\{1 - \exp\left[-2.91\left(\frac{\theta-\theta_0}{\Delta\theta_2}\right)^{1.66+1}\right]\right\} \quad (8)$$

$$x_b(\theta) = 0.29\left\{1 - \exp\left[-2.25\left(\frac{\theta-\theta_0}{\Delta\theta_1}\right)^{0.16+1}\right]\right\} + 0.71\left\{1 - \exp\left[-2.25\left(\frac{\theta-\theta_0}{\Delta\theta_2}\right)^{2.21+1}\right]\right\} \quad (9)$$

Table 6 Coefficients for form factor reduced double Wiebe function

	λ	a_1	M	a_2
Data 1	0.13	9.59	1.84	4.47
Data 2	0.13	9.24	1.91	3.83
Data 3	0.12	8.53	1.89	2.45
Data 4	0.13	8.95	1.68	2.50
Data 5	0.13	8.48	1.63	2.46
Data 6	0.12	8.09	1.58	2.45
Data 7	0.13	8.29	1.50	2.73
Data 8	0.13	8.27	1.44	2.65
Data 9	0.12	8.34	1.45	2.61

Table 7 Coefficients for efficiency factor reduced double Wiebe function

	λ	a	m_1	m_2
Data 1	0.33	2.39	0.11	2.54
Data 2	0.28	2.37	0.21	2.47
Data 3	0.28	2.09	0.25	2.49
Data 4	0.28	2.18	0.11	2.23
Data 5	0.30	2.16	0.17	2.22
Data 6	0.30	2.14	0.21	2.14
Data 7	0.28	2.41	0.13	1.97
Data 8	0.29	2.29	0.13	1.92
Data 9	0.28	2.20	0.13	1.93

Table 8 RMSE for single and double Wiebe functions

	SWF	DDWF	RDWF-form factor	RDWF-efficiency factor
Data 10	8.6%	2.1%	2%	2.1%
Data 11	8.3%	0.8%	1.3%	0.8%
Data 12	5.1%	0.7%	1.1%	0.7%

Heat Release and Cylinder Pressure Simulation Result. The heat release fraction during the combustion process was calculated from the experimental data using our in-house heat release analysis code. This MFB curve was used as inputs to fit the coefficients of the single and double Wiebe functions. The most appropriate function was selected for operating points 1 through 9, shown in Table 3. Operating points 10–12, shown in Table 3, were used as validation cases. The computational 1D system-level simulation model results are presented in this section.

Figures 4–6 illustrate the normalized heat release rate from the experiments, with syngas and anode off-gas at different compression ratios, compared with the estimated MFB using Eqs. (6)–(9). The MFB of the single Wiebe function resulted in a significant mismatch at the main combustion section compared with the experimental results. Both the detailed double Wiebe function and the efficiency factor reduced double Wiebe functions had the least error. In particular, the form factor reduced double Wiebe function resulted in a reasonable agreement with the experimental data. Meanwhile, by comparing the combustion phasing it is clear that the double Wiebe function was able to capture the combustion timing more accurate than the single Wiebe function. The combustion timing for detailed and reduced double Wiebe function are very close. The detailed information of the combustion

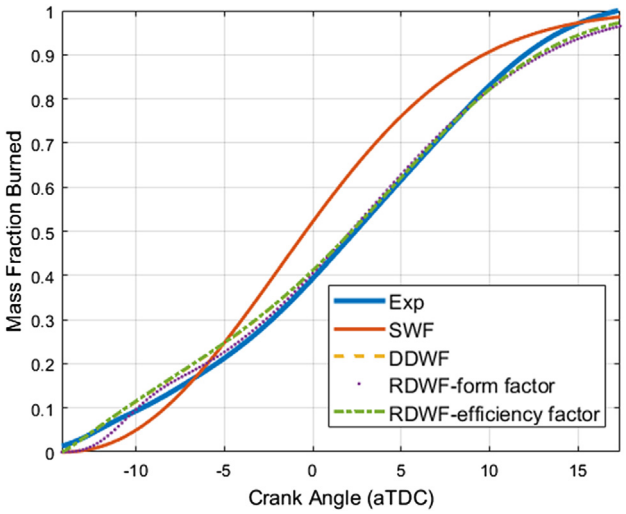

Fig. 4 Experiment and predicted MFB at CR = 9 using syngas

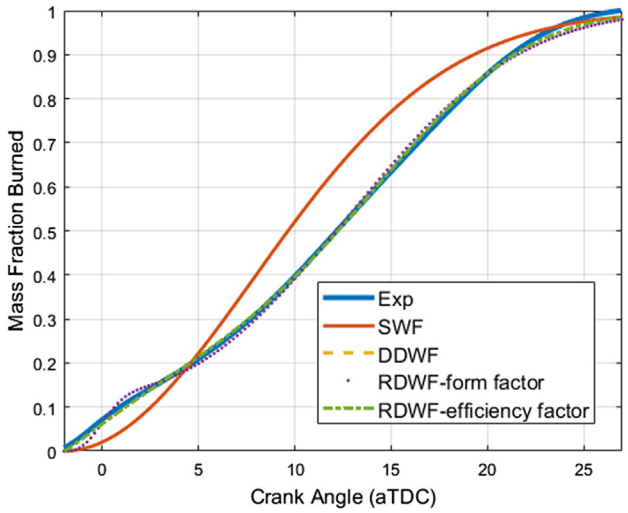

Fig. 5 Experiment and predicted MFB at CR = 11 using syngas

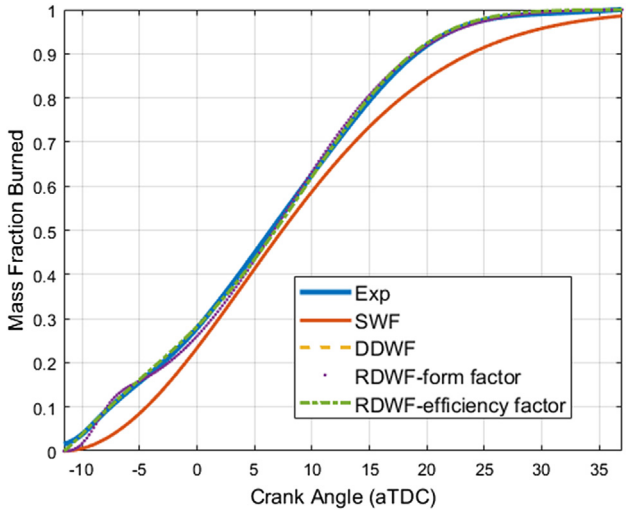

Fig. 6 Experiment and predicted MFB at CR = 11 using anode off-gas

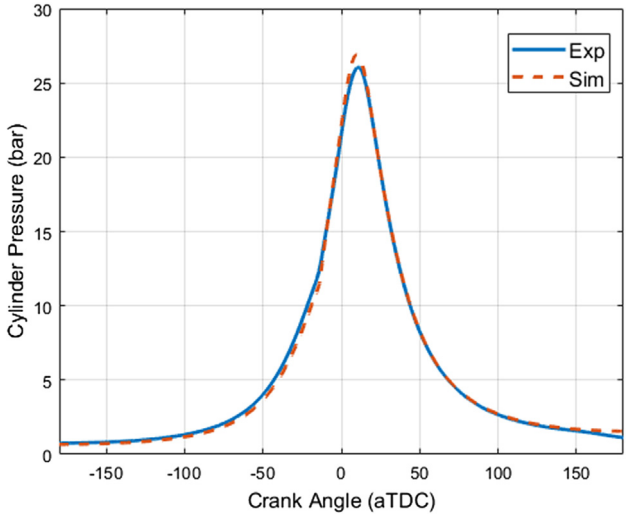

Fig. 7 Experiment and modeling pressure at CR = 9 using syngas

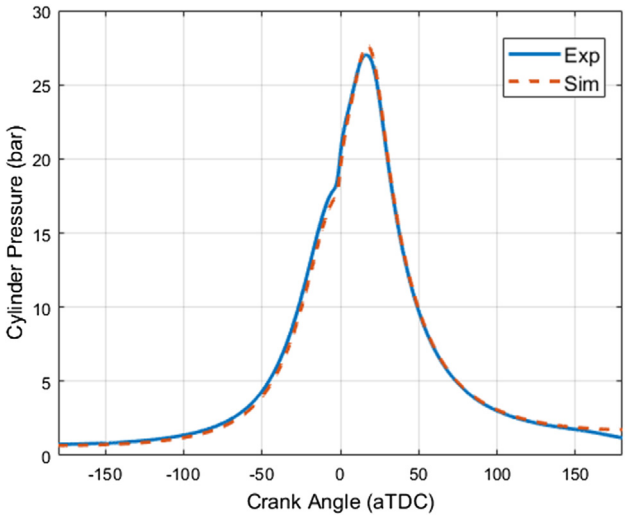

Fig. 8 Experiment and modeling pressure at CR = 11 using syngas

phasing for the experiment and predicted combustion profiles were shown in Appendix A. Considering the tradeoff between accuracy and the complexity of the algorithm, the results show that the efficiency factor reduced double Wiebe function can be considered as the best option to predict SI combustion using syngas and anode off-gas as the fuel.

Looking more closely at the efficiency factor reduced double Wiebe function, as shown in Eq. (9), the weight factor is 0.29, which means more combustion occurs at the diffusion combustion stage than the premixed combustion stage. This is attributed to the higher laminar flame speed of the H_2 in the fuel content of both syngas and anode off-gas, which is beneficial for flame propagation in SI combustion. The form factor for the two combustion stages is 0.16 and 2.21, which means that combustion in the two stages is fast, but not symmetric. At the beginning of the combustion process, there is a mismatch between the predicted curve and the calculated result, which is due to the assumption that the premixed and diffusion combustion starts at the same crank angle position while that is not physically the case. The efficiency factor is 2.25, which suggests that a short combustion duration occurs in the cylinder. From Figs. 4–6, it is also apparent that the MFB

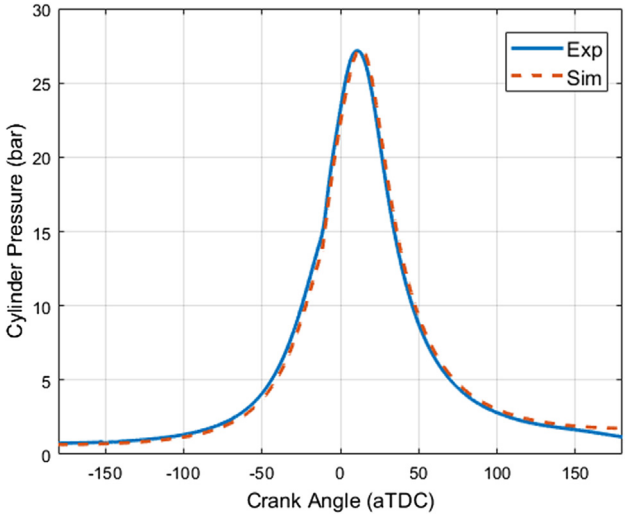

Fig. 9 Experiment and modeling pressure at CR = 11 using anode off-gas

curves are sharply increasing between the start of combustion and the 95% of total fuel burned.

Figures 7–9 compare experimental and simulated cylinder pressures for three cases using the RDWF-efficiency factor. In these three figures, slight mismatches appear close to top dead center due to the discrepancy between the experimental data and the predicted MFB at the start of combustion. The simulated pressure trace at the expansion stroke is higher than the measurement due to the delay of the burned fuel fraction. Generally, the mismatch between the experiments and the simulation results is negligible, which validates that the one-dimensional model with the specific double Wiebe function can be used to estimate the combustion process of a SI engine fueled with both syngas and anode off-gas. Hence, this model has the potential for detailed studies of general SI combustion with syngas-based fuels.

Conclusions

This study has explored the potential use of alternative Wiebe functions to describe the apparent heat release from SI combustion using syngas and anode off-gas as fuels. A single Wiebe function and three double Wiebe functions were developed based on measured heat release data and compared. The functions were subsequently embedded in a one-dimensional engine system-level model to predict performance for different engine geometry and operating conditions. Based on the discussion in the previous sections, the following conclusions can be drawn

- The single Wiebe function can capture combustion with low accuracy. Hence, SI combustion using syngas and anode off-gas cannot be represented by a governing function.
- The detailed double Wiebe function is able to predict the syngas and anode off-gas SI combustion with the highest accuracy.
- The RDWF-efficiency factor can describe syngas and anode off-gas heat release almost as precisely as the detailed double Wiebe function.
- The RDWF-form factor model produces some discrepancies against experimental data at the main heat release section.
- The one-dimensional system-level model, using an RDWF-efficiency factor heat release description, can be used to analyze both the syngas SI combustion and anode off-gas SI combustion for future studies.

Acknowledgment

The authors would like to thank AVL for their generous technical support and academic licenses granted for the use of AVL BOOST.

Funding Data

- Advanced Research Projects Agency-Energy (ARPA-E) (Award ID: AR0000959; Funder ID: 10.13039/100006133).

Nomenclature

aTDC = after the top dead center
bTDC = before the top dead center
CA0 = crank angle degree of 0% heat release
CA95 = crank angle degree of 95% heat release
CAD = crank angle degree
CR = compression ratio
DDWF = detailed double Wiebe Function
LSE = least square error
MFB = mass fraction burned
RCCI = reactivity controlled compression ignition
SOC = start of combustion
SOFC = solid oxide fuel cell
SWF = single Wiebe function
RDWF = reduced double Wiebe function
RMSE = root mean square error

Appendix A

Table 9 Combustion phasing for (*a*) experimental data, (*b*) single Wiebe function, (*c*) detailed double Wiebe function, (*d*) form factor reduced double Wiebe function, and (*e*) efficiency factor reduced double Wiebe function

(*a*)

Data	CA10 (deg aTDC)	CA50 (deg aTDC)	CA90 (deg aTDC)
1	−2	7	17
2	−6	4	14
3	−8	3	14
4	−2	10	22
5	−6	7	21
6	−9	5	19
7	−8	7	23
8	−8	7	24
9	−10	6	23
10	−10	2	14
11	1	12	23
12	−8	6	22

(*b*)

Data	CA10 (deg aTDC)	CA50 (deg aTDC)	CA90 (deg aTDC)
1	2	12	29
2	−2	7	22
3	−6	1	13
4	−1	7	21
5	−4	4	19
6	−7	2	18
7	−6	5	23
8	−6	4	23
9	−8	3	22
10	−8	0	13
11	3	10	22
12	−4	7	29

(*c*)

Data	CA10 (deg aTDC)	CA50 (deg aTDC)	CA90 (deg aTDC)
1	−2	7	17
2	−6	4	15
3	−8	3	15
4	−2	10	23
5	−5	8	21
6	−9	5	20
7	−8	7	23
8	−8	7	23
9	−10	6	23
10	−11	2	15
11	1	12	24
12	−8	7	22

(*d*)

Data	CA10 (deg aTDC)	CA50 (deg aTDC)	CA90 (deg aTDC)
1	−2	7	18
2	−6	4	16
3	−8	3	15
4	−3	10	23
5	−6	7	22
6	−9	5	20
7	−8	7	23
8	−8	7	24
9	−10	6	23
10	−10	2	16
11	1	12	24
12	−8	7	22

Table 9 (Continued)

(*e*)

Data	CA10 (deg aTDC)	CA50 (deg aTDC)	CA90 (deg aTDC)
1	−2	7	17
2	−6	4	15
3	−8	3	15
4	−2	10	23
5	−5	8	21
6	−9	5	20
7	−8	7	23
8	−8	7	23
9	−10	6	23
10	−11	2	15
11	1	12	24
12	−8	7	22

Appendix B

Table 10 Spark timing, combustion timing, and combustion duration for experimental data

Data	Spark timing (deg aTDC)	Start of combustion (deg aTDC)	Combustion duration (deg)
1	−9	−5	19
2	−13	−9	20
3	−16	−12	21
4	−10	−6	25
5	−14	−9	26
6	−18	−13	28
7	−14	−12	30
8	−14	−12	32
9	−16	−14	32
10	−19	−14	24
11	−6	−2	22
12	−22	−12	30

References

[1] Ayala, F. A., Gerty, M. D., and Heywood, J., 2006, "Effects of Combustion Phasing, Relative Air-Fuel Ratio, Compression Ratio, and Load on SI Engine Efficiency," SAE Paper No. 2006-01-0229, pp. 177–195.

[2] Ayala, F. A., and Heywood, J. B., 2007, "Lean SI Engines: The Role of Combustion Variability in Defining Lean Limits," SAE Paper No. 2007-24-0030.

[3] Chaichan, M., 2012, "Characterization of Lean Misfire Limits of Mixture Alternative Gaseous Fuels Used for Spark Ignition Engines," Tikrit J. Eng. Sci., **19**(1), pp. 50–61.

[4] Guerra, L., Moura, K., Rodrigues, J., Gomes, J., Puna, J., Bordado, J., and Santos, T., 2018, "Synthesis Gas Production From Water Electrolysis, Using the Electrocracking Concept," J. Environ. Chem. Eng., **6**(1), pp. 604–609.

[5] Raman, P., and Ram, N. J. E., 2013, "Performance Analysis of an Internal Combustion Engine Operated on Producer Gas, in Comparison With the Performance of the Natural Gas and Diesel Engines," Energy, **63**, pp. 317–333.

[6] Bauer, C., and Forest, T., 2001, "Effect of Hydrogen Addition on the Performance of Methane-Fueled Vehicles. Part I: Effect on SI Engine Performance," Int. J. Hydrogen Energy, **26**(1), pp. 55–70.

[7] Furuhama, S., 1983, "State of the Art and Future Trends in Hydrogen-Fuelled Engines," Int. J. Veh. Des., **4**(4), pp. 359–385.

[8] Karim, G., 2003, "Hydrogen as a Spark Ignition Engine Fuel," Int.J. Hydrogen Energy, **28**(5), pp. 569–577.

[9] Sridhar, G., and Yarasu, R. B., 2010, *Facts About Producer Gas Engine*, Paths to Sustainable Energy, Ng, A., ed., INTECH Open Access Publisher, Greenville, SC.

[10] Ran, Z., Hariharan, D., Lawler, B., and Mamalis, S., 2019, "Experimental Study of Lean Spark Ignition Combustion Using Gasoline, Ethanol, Natural Gas, and Syngas," Fuel, **235**, pp. 530–537.

[11] Ran, Z., Hariharan, D., Lawler, B., and Mamalis, S., 2020, "Exploring the Potential of Ethanol, CNG, and Syngas as Fuels for Lean Spark-Ignition combustion-An Experimental Study," Energy, **191**, p. 116520.

[12] Mustafi, N., Miraglia, Y. C., Raine, R. R., Bansal, P. K., and Elder, S. T., 2006, "Spark-Ignition Engine Performance With 'Powergas' Fuel (Mixture of CO/H_2): A Comparison With Gasoline and Natural Gas," Fuel, **85**(12–13), pp. 1605–1612.

[13] Bika, A. S., Franklin, L., and Kittelson, D., 2011, "Engine Knock and Combustion Characteristics of a Spark Ignition Engine Operating With Varying Hydrogen and Carbon Monoxide Proportions," Int. J. Hydrogen Energy, **36**(8), pp. 5143–5152.

[14] Dai, X., Ji, C., Wang, S., Liang, C., Liu, X., and Ju, B., 2012, "Effect of Syngas Addition on Performance of a Spark-Ignited Gasoline Engine at Lean Conditions," Int. J. Hydrogen Energy, **37**(19), pp. 14624–14631.

[15] Shah, A., Srinivasan, R., Filip To, R. D., and Columbus, E. P., 2010, "Performance and Emissions of a Spark-Ignited Engine Driven Generator on Biomass Based Syngas," Bioresour. Technol., **101**(12), pp. 4656–4661.

[16] Longwell, J. P., Rubin, E. S., and Wilson, J., 1995, "Coal: Energy for the Future," Prog. Energy Combust. Sci., **21**(4), pp. 269–360.

[17] Bizon, N., and Thounthong, P., 2018, "Fuel Economy Using the Global Optimization of the Fuel Cell Hybrid Power Systems," Energy Convers. Manage., **173**, pp. 665–678.

[18] Vora, S. D., 2014, "Office of Fossil Energy's Solid Oxide Fuel Cell Program Overview," 15th Annual SECA Workshop, Pittsburgh, PA, July 22–23, pp. 22–23.

[19] Fyffe, J. R., Donohue, M. A., Regalbuto, M. C., and Edwards, C. F., 2017, "Mixed Combustion–Electrochemical Energy Conversion for High-Efficiency, Transportation-Scale Engines," Int. J. Engine Res., **18**(7), pp. 701–716.

[20] Kim, J., Kim, Y., Choi, W., Ahn, K. Y., and Song, H. H., 2020, "Analysis on the Operating Performance of 5-kW Class Solid Oxide Fuel Cell-Internal Combustion Engine Hybrid System Using Spark-Assisted Ignition," Appl. Energy, **260**, p. 114231.

[21] Ran, Z., Assanis, D., Hariharan, D., and Mamalis, S., 2020, "Experimental Study of Spark-Ignition Combustion Using the Anode Off-Gas From a Solid Oxide Fuel Cell," SAE Paper No. 2020-01-0351.

[22] Heywood, J. B., 2018, *Internal Combustion Engine Fundamentals*, McGraw-Hill Education, New York.

[23] Heywood, J. B., Higgins, J. M., Watts, P. A., and Tabaczynski, R. J., 1979, "Development and Use of a Cycle Simulation to Predict SI Engine Efficiency and NOx Emissions," SAE Paper No. 790291.

[24] Borg, J. M., and Alkidas, A. C., 2008, "Investigation of the Effects of Autoignition on the Heat Release Histories of a Knocking SI Engine Using Wiebe Functions," SAE Paper No. 2008-01-1088.

[25] Shivapuji, A. M., and Dasappa, S., 2013, "Experiments and Zero D Modeling Studies Using Specific Wiebe Coefficients for Producer Gas as Fuel in Spark-Ignited Engines," Archive Proc. Inst. Mech. Eng., Part C, **227**(3), pp. 504–519.

[26] Carrera, J., Riesco-Ávila, J. M., Martinez-Martinez, S., Sánchez-Cruz, F. A., and Gallegos-Muñoz, A., 2013, "Numerical Study on the Combustion Process of a Biogas Spark-Ignition Engine," Them. Sci., **17**(1), pp. 241–254.

[27] Ghojel, J. I., 1982, "A Study of Combustion Chamber Arrangements and Heat Release in DI Diesel Engines," SAE Paper No. 821034.

[28] Yasar, H., Soyhan, H. S., Walmsley, H., Head, B., and Sorusbay, C., 2008, "Double-Wiebe Function: An Approach for Single-Zone HCCI Engine Modeling," Appl. Therm. Eng., **28**(11–12), pp. 1284–1290.

[29] Aziz, A. R. A., and Heikal, M., 2013, "Double Stage Wiebe: An Approach to Single Zone Modeling of Dual Fuel HCCI Combustion," Asian J. Sci. Res., **6**(2), pp. 388–394.

[30] Yeliana, Y., Cooney, C., Worm, J., Michalek, D. J., and Naber, J. D., 2011, "Estimation of Double-Wiebe Function Parameters Using Least Square Method for Burn Durations of Ethanol-Gasoline Blends in Spark Ignition Engine Over Variable Compression Ratios and EGR Levels," Appl. Therm. Eng., **31**(14–15), pp. 2213–2220.

[31] Liu, J., and Dumitrescu, C., 2019, "Single and Double Wiebe Function Combustion Model for a Heavy-Duty Diesel Engine Retrofitted to Natural-Gas Spark-Ignition," Appl. Energy, **248**, pp. 95–103.

[32] Ran, Z., Longtin, J., and Assanis, D., "Investigating Anode Off-Gas Under Spark-Ignition Combustion for SOFC-ICE Hybrid Systems," Int. J. Engine Res., **23**(5), pp. 830–845.

[33] AVL BOOST, 2013, Theory version 2013.2, AVL LIST GmbH, Graz, Austria.